Further development of the improved quantum molecular dynamics model and its application to fusion reactions near the barrier

Ning Wang,[1,2,*] Zhuxia Li,[1,2,3,†] Xizhen Wu,[1,3,†] Junlong Tian,[1] YingXun Zhang,[1] and Min Liu[1]
[1]*China Institute of Atomic Energy, P. O. Box 275(18), Beijing 102413, People's Republic of China*
[2]*Institute of Theoretical Physics, Chinese Academy of Sciences, Beijing 100080, People's Republic of China*
[3]*Nuclear Theory Center of National Laboratory of Heavy Ion Accelerator, Lanzhou 730000, People's Republic of China*
(Received 23 October 2003; published 17 March 2004)

The improved quantum molecular dynamics model is further developed by introducing new parameters in interaction potential energy functional based on Skyrme interaction of SkM* and SLy series. The properties of ground states of selected nuclei can be reproduced very well. The Coulomb barriers for a series of reaction systems are studied and compared with the results of the proximity potential. The fusion excitation functions for a series of fusion reactions are calculated and the results are in good agreement with experimental data.

DOI: 10.1103/PhysRevC.69.034608 PACS number(s): 25.70.−z, 24.10.−i

I. INTRODUCTION

Recently, the study of the mechanism for heavy-ion fusion reactions at energies near the Coulomb barrier, especially, the mechanism for the enhancement of fusion cross sections for neutron-rich systems has attracted a lot of attention. The knowledge of the mechanism of the enhancement of fusion cross sections for heavy and neutron-rich systems is useful in the synthesis of superheavy elements. In heavy-ion fusion reactions, the excitation and deformation of projectile and target, neck formation, and nucleon transfer strongly influence the dynamics of fusion processes. These effects are more pronounced near and below the fusion barrier. For heavy systems, in order to consider these effects a very large number of degrees of freedom of motion is involved and the situation becomes very complicated. Thus one will meet great difficulty by macroscopic dynamics models [1] in which only few degrees of freedom of motion are included. The difficulty is also encountered by the fusion coupled channel model [2] for it is quite difficult, even impossible, to include such a large number of possible channels in practical calculations. Therefore, it is highly requisite to develop a microscopic dynamical model suitable for studying heavy-ion fusion reactions by which one can consistently take account of the dynamical deformation, particle transfer, isospin, and mass asymmetry effects, etc. In our previous work [3,4], an improved quantum molecular dynamics (ImQMD) model was proposed. Main improvements in the ImQMD model are as follows: The surface and surface symmetry energy terms are introduced in the potential energy part; a system size dependent wave-packet width is introduced in order to consider the evolution of the wave-packet width; an approximate treatment of antisymmetrization, namely, a phase space occupation constraint is adopted [5]. With this model we have studied the dynamical evolution of the fusion barrier as well as the development of the neck in fusion reactions of ^{40,48}Ca+^{90,96}Zr. However, more tests of our model are needed. Before that one of the most urgent problems that has to be solved is to increase the time of keeping an individual nucleus to be stable and in a good shape (close to ground state shape) without emission of nucleons in order to study the dynamical process for fusion reactions of heavy nuclei. As is well known that the time scale for the formation process of a compound system in a fusion reaction of heavy nuclei is about thousands fm/c, and also the time scale of quasifission which reduces the fusion probability substantially in fusion processes of heavy nuclei is about several thousands fm/c or longer. To meet this requirement, in this paper we develop an updated version of improved quantum molecular dynamics model named ImQMD-II based on our previous work [3,4]. This paper we mainly devote to modification of the parameters of the potential energy functional in the model. As is well known that the parameters of the potential energy functional in the QMD model are obtained based on Skyrme forces. There are quite a lot of new versions of Skyrme forces having been developed following the development of the knowledge of nuclear equation of state. The newly developed Skyrme forces such as the SLy series are designed to study the properties of nuclei away from the β-stability line in addition to nuclei along the β-stability line. It has been shown that these modern Skyrme forces can describe the properties of the nuclei away from β-stability line better than the old Skyrme forces [6]. Therefore it seems to us to be worthwhile to try new parameters for the ImQMD model based on the modern parametrizations of Skyrme forces such as the SLy series as well as the other popular versions.

The paper is organized as follows. In Sec. II, we briefly introduce the formalism of the ImQMD-II model and the improvements. The applications of this model to the fusion reactions at energies near the Coulomb barrier are reported in Sec. III. Finally, the summary and discussion are given in Sec. IV.

II. FURTHER DEVELOPMENT OF THE IMPROVED QMD MODEL

In this section we introduce the updated ImQMD model (ImQMD-II) in more details. First, a brief introduction to the

*Electronic address: wangning@itp.ac.cn
†Electronic address: lizwux@iris.ciae.ac.cn

ImQMD model is presented. Then, we will give the new development of ImQMD. Finally, the calculation results of the properties of selected nuclei with the ImQMD-II model are given.

A. Brief introduction of the ImQMD model

For readers convenience, let us first briefly introduce the ImQMD model. In the ImQMD model, the same as in the original QMD model [7–10], each nucleon is represented by a coherent state of a Gaussian wave packet

$$\phi_i(\mathbf{r}) = \frac{1}{(2\pi\sigma_r^2)^{3/4}}\exp\left[-\frac{(\mathbf{r}-\mathbf{r}_i)^2}{4\sigma_r^2} + \frac{i}{\hbar}\mathbf{r}\cdot\mathbf{p}_i\right], \quad (1)$$

where $\mathbf{r}_i, \mathbf{p}_i$, are the centers of ith wave packet in the coordinate and momentum space, respectively. σ_r represents the spatial spread of the wave packet. The total N-body wave function is assumed to be the direct product of these coherent states. Through a Wigner transformation, the one-body phase space distribution function for N-distinguishable particles is given by:

$$f(\mathbf{r},\mathbf{p}) = \sum_i \frac{1}{(\pi\hbar)^3}\exp\left[-\frac{(\mathbf{r}-\mathbf{r}_i)^2}{2\sigma_r^2} - \frac{2\sigma_r^2}{\hbar^2}(\mathbf{p}-\mathbf{p}_i)^2\right]. \quad (2)$$

For identical fermions, the effects of the Pauli principle were discussed in a broader context by Feldmeier and Schnack [11]. The approximate treatment of antisymmetrization is adopted in the ImQMD model by means of the phase space occupation constraint method [3–5]. The density and momentum distribution functions of a system read

$$\rho(\mathbf{r}) = \int f(\mathbf{r},\mathbf{p})d^3p = \sum_i \rho_i(\mathbf{r}), \quad (3)$$

$$g(\mathbf{p}) = \int f(\mathbf{r},\mathbf{p})d^3r = \sum_i g_i(\mathbf{p}), \quad (4)$$

respectively, where the sum runs over all particles in the system. $\rho_i(\mathbf{r})$ and $g_i(\mathbf{p})$ are the density and momentum distributions of nucleon i:

$$\rho_i(\mathbf{r}) = \frac{1}{(2\pi\sigma_r^2)^{3/2}}\exp\left[-\frac{(\mathbf{r}-\mathbf{r}_i)^2}{2\sigma_r^2}\right], \quad (5)$$

$$g_i(\mathbf{p}) = \frac{1}{(2\pi\sigma_p^2)^{3/2}}\exp\left[-\frac{(\mathbf{p}-\mathbf{p}_i)^2}{2\sigma_p^2}\right], \quad (6)$$

where σ_r and σ_p are the widths of wave packets in coordinate and momentum space, respectively, and they satisfy the minimum uncertainty relation:

$$\sigma_r\sigma_p = \frac{\hbar}{2}. \quad (7)$$

The propagation of nucleons under the self-consistently generated mean field is governed by Hamiltonian equations of motion:

$$\dot{\mathbf{r}}_i = \frac{\partial H}{\partial \mathbf{p}_i}, \quad \dot{\mathbf{p}}_i = -\frac{\partial H}{\partial \mathbf{r}_i}. \quad (8)$$

The Hamiltonian H consists of the kinetic energy and the effective interaction potential energy:

$$H = T + U, \quad (9)$$

$$T = \sum_i \frac{\mathbf{p}_i^2}{2m}. \quad (10)$$

The effective interaction potential energy includes the nuclear local interaction potential energy and the Coulomb interaction potential energy:

$$U = U_{loc} + U_{Coul}, \quad (11)$$

and

$$U_{loc} = \int V_{loc}(\mathbf{r})d\mathbf{r}, \quad (12)$$

where $V_{loc}(\mathbf{r})$ is potential energy density.

The potential energy density $V_{loc}(\mathbf{r})$ in the ImQMD model reads

$$V_{loc} = \frac{\alpha}{2}\frac{\rho^2}{\rho_0} + \frac{\beta}{\gamma+1}\frac{\rho^{\gamma+1}}{\rho_0^\gamma} + \frac{g_{sur}}{2\rho_0}(\nabla\rho)^2 + g_\tau\frac{\rho^{\eta+1}}{\rho_0^\eta} + \frac{C_s}{2\rho_0}[\rho^2 - \kappa_s(\nabla\rho)^2]\delta^2, \quad (13)$$

where $\delta = \rho_n - \rho_p/\rho_n + \rho_p$. The first three terms in above expression can be obtained from the potential energy functional of Skyrme forces directly. The fifth term is the symmetry potential energy part where both the bulk and the surface symmetry energy are included. In addition, we introduce an extra small correction term $V_\tau = g_\tau\rho^{\eta+1}/\rho_0^\eta$ (named tau term) in the potential energy functional. Inserting expression (13) into (12), we obtain the local interaction potential energy omitting self-energies:

TABLE I. Parameters used in the QMD model and the corresponding values obtained from various Skyrme parametrizations.

Parameter	α (MeV)	β (MeV)	γ	g_{sur} (MeV fm^2)
QMD (hard)	−124.0	71.0	2	
QMD (soft)	−356.0	303.0	7/6	
SIII [15]	−139.6	71.4	2	20.14
SkP [18]	−362.8	309.6	7/6	19.84
SkM [16]	−327.3	258.0	7/6	20.32
SkM* [17]	−327.3	258.0	7/6	21.82
SLy10 [6]	−310.2	228.8	7/6	21.57

TABLE II. The parameters of IQ1.

Parameter	α (MeV)	β (MeV)	γ	g_0 (MeV fm^2)	g_τ (MeV)	η	C_s (MeV)	κ_s (fm^2)	ρ_0 (fm^{-3})
IQ1	−310.0	258.0	7/6	19.8	9.5	2/3	32.0	0.08	0.165

$$U_{loc} = \frac{\alpha}{2}\sum_i \sum_{j\neq i} \frac{\rho_{ij}}{\rho_0} + \frac{\beta}{\gamma+1}\sum_i \left(\sum_{j\neq i}\frac{\rho_{ij}}{\rho_0}\right)^{\gamma} + \frac{g_0}{2}\sum_i \sum_{j\neq i} f_{sij}\frac{\rho_{ij}}{\rho_0} + g_\tau \sum_i \left(\sum_{j\neq i}\frac{\rho_{ij}}{\rho_0}\right)^{\eta} + \frac{C_s}{2}\sum_i \sum_{j\neq i} t_i t_j \frac{\rho_{ij}}{\rho_0}(1-\kappa_s f_{sij}), \quad (14)$$

where

$$\rho_{ij} = \frac{1}{(4\pi\sigma_r^2)^{3/2}}\exp\left[-\frac{(\mathbf{r}_i-\mathbf{r}_j)^2}{4\sigma_r^2}\right], \quad (15)$$

$$f_{sij} = \frac{3}{2\sigma_r^2} - \left(\frac{\mathbf{r}_i-\mathbf{r}_j}{2\sigma_r^2}\right)^2, \quad (16)$$

and $t_i=1$ for protons and -1 for neutrons. One should note that the third term in Eq. (14) comes from both surface term and the correction to the second term of Eq. (13) (see Ref. [3]), and thus g_0 is actually treated as a parameter in the model.

The Coulomb energy can be written as a sum of the direct and the exchange contribution, and the latter being taken into account in the Slater approximation [12–14]

$$U_{Coul} = \frac{1}{2}\int \rho_p(\mathbf{r})\frac{e^2}{|\mathbf{r}-\mathbf{r}'|}\rho_p(\mathbf{r}')d\mathbf{r}d\mathbf{r}' - e^2\frac{3}{4}\left(\frac{3}{\pi}\right)^{1/3}\int \rho_p^{4/3}d\mathbf{R}, \quad (17)$$

where ρ_p is the density distribution of protons of the system. The collision term and phase space occupation constraint can also readjust the momenta, but the former plays a very small role in low energy heavy-ion collisions and the latter only happens occasionally. The phase space occupation constraint method [5] and the system-size-dependent wave-packet width are adopted as that in the previous version of ImQMD [3,4].

B. The new development in ImQMD(ImQMD-II) model

The new development of the ImQMD model mainly are reconsidering the parameters in the potential energy functional [see expression (13)]. In the expression (13), the first three terms can be obtained from the potential energy functional of a standard Skyrme interaction directly. The parameters α, β, γ, and g_{sur} can be related to the parameters of Skyrme interactions by

$$\frac{\alpha}{2}\frac{1}{\rho_0} = \frac{3}{8}t_0, \quad (18)$$

$$\frac{\beta}{\gamma+1}\frac{1}{\rho_0^{\gamma}} = \frac{1}{16}t_3, \quad (19)$$

and

$$\frac{g_{sur}}{2\rho_0} = \frac{1}{64}(9t_1 - 5t_2 - 4t_2x_2), \quad (20)$$

where the parameter γ takes the same value as in the Skyrme interaction. The linear density dependence of the symmetry energy term is taken and the parameter is fixed by the symmetry energy coefficient. In Table I we list the α, β, and γ parameters used in the QMD model [8] and the corresponding values obtained from various versions of Skyrme interaction [6,15–18]. From the table one can find the parameters of QMD(hard) are close to that of SIII, and the soft one is close to SkP.

The SIII parametrization was proposed in 1975 and with it one could describe the ground state properties of spherical nuclei very well. However, the incompressibility modulus of symmetric nuclear matter obtained from SIII ($K_\infty \approx 365$ MeV) is too high [19]. Taking this into account, Krivine *et al.* derived the SkM interaction at 1980. Later on, detailed studies of the fission barriers [20] in the actinide region resulted in a more refined value of the nuclear surface tension. Then SkM* [17] was derived which gave a more refined surface tension. Nowadays, the symmetry energy part of the interaction attracts a lot of interest as nuclei further away from the stability line can be expected to be produced with the coming radioactive beam facilities. Putting more emphasis on the isospin degree of freedom, a series of sets of SLy parametrizations were proposed in the late 1990's for

TABLE III. The binding energies and root-mean-square charge radii of a series ground state nuclei calculated by the ImQMD-II model with IQ1 interaction.

Nuclei		^{208}Pb	^{140}Ce	^{132}Sn	^{114}Sn	^{90}Zr	^{56}Ni	^{48}Ca	^{40}Ca	^{16}O
Binding	Expt. [17] (MeV)	7.87	8.38	8.35	8.53	8.71	8.64	8.67	8.55	7.98
energy	IQ1 (MeV)	7.77	8.35	8.27	8.51	8.71	8.63	8.67	8.65	8.23
rms	Expt. [17] (fm)	5.50	4.88			4.27	3.75	3.48	3.49	2.73
radius	IQ1 (fm)	5.51	4.87	4.79	4.55	4.25	3.71	3.54	3.44	2.72

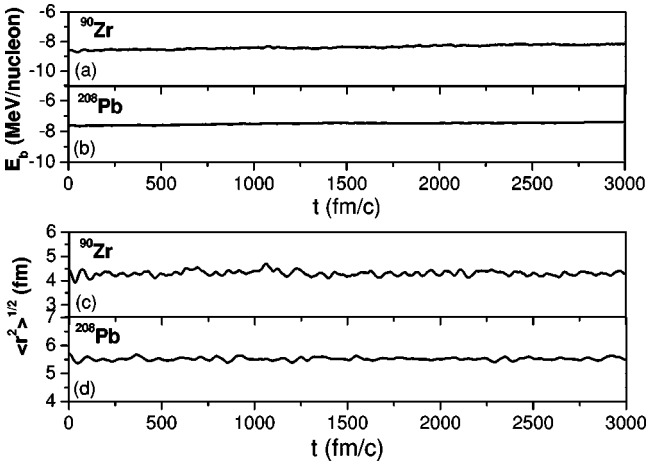

FIG. 1. The time evolution of binding energies and root-mean-square charge radii for ^{90}Zr and ^{208}Pb calculated by the ImQMD-II model with parameter set of IQ1.

reproducing the properties of the nuclei from the β-stability line to the drip lines [6].

Considering the successes of SkM* in describing the surface tension and SLy in describing the properties of nuclear systems far away from β-stability line, the SkM* and SLy parametrization can provide us with a reference to adjust the new ImQMD parameters. Concerning the symmetry energy term, the linear density dependence of the bulk symmetry energy term is taken and the parameter is fixed by the symmetry energy coefficient. The surface-symmetry energy term is also introduced. This term is important for having a correct neutron skin, which was introduced in the liquid-drop model [21,22]. For Skyrme interactions [6,23], the surface-symmetry term can be extracted which reads

$$U_{surf-symm} = -\frac{C_s \kappa_s}{2\rho_0} \int [\nabla \rho(\mathbf{r})]^2 \delta(\mathbf{r})^2 d\mathbf{r}. \quad (21)$$

It modifies the symmetry potential at surface region, and therefore it is especially important for correctly describing the neck dynamics in fusion reactions of neutron-rich nuclei. In our previous work this term was introduced and it was found that this term played a role in the fusion dynamics. We will study this effect in the following section. Taking SkM* and SLy parametrizations as the reference we propose a new set of parameters for the ImQMD model by reproducing the properties of ground state of selected nuclei ^{208}Pb, ^{90}Zr, ^{40}Ca, and ^{16}O and the fusion cross sections of ^{40}Ca $+^{48}$Ca [24], ^{40}Ca$+^{90,96}$Zr [25]. The new set of ImQMD parameters named IQ1 is listed in Table II.

From Tables I and II, one can see that the parameter set of IQ1 is generally close to SLy10 and SkM*.

In Table III we list the binding energies and the root-mean-square charge radii of ^{208}Pb, ^{140}Ce, ^{132}Sn, ^{114}Sn, ^{90}Zr, ^{56}Ni, ^{46}Ca, ^{40}Ca, and ^{16}O calculated by the ImQMD-II model with parameter set IQ1. The experimental data are also listed for comparison and it is shown that the calculated results are in good agreement with experimental data. In Fig. 1, we present the time evolution of binding energies and root-mean-square charge radii for ^{90}Zr and ^{208}Pb calculated by the ImQMD-II model with IQ1 parameters. One can see that their binding energies and root-mean-square charge radii remain constant with a very small fluctuation and the bound nuclei evolve stably without spurious emission for a period of time of about 3000 fm/c, which is essential for applications to fusion reactions of heavy nuclei as is discussed in the introduction.

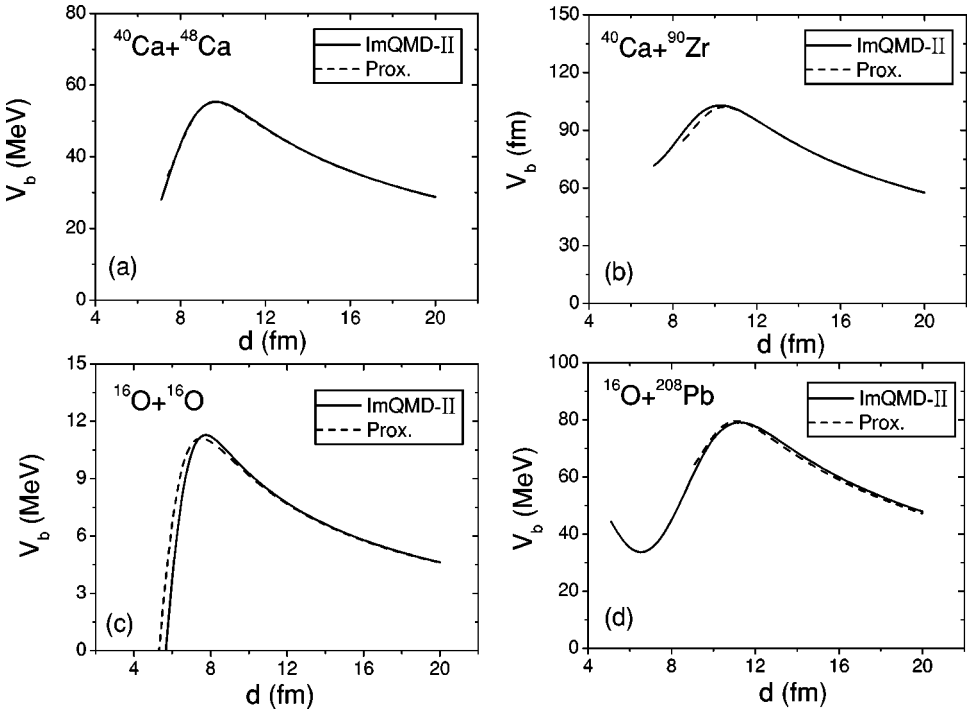

FIG. 2. The static Coulomb barriers of ^{40}Ca$+^{48}$Ca, ^{40}Ca $+^{90}$Zr, ^{16}O$+^{16}$O, and ^{16}O$+^{208}$Pb. The solid and dashed curves denote the results of ImQMD-II with parameters of IQ1 and those of proximity potential, respectively.

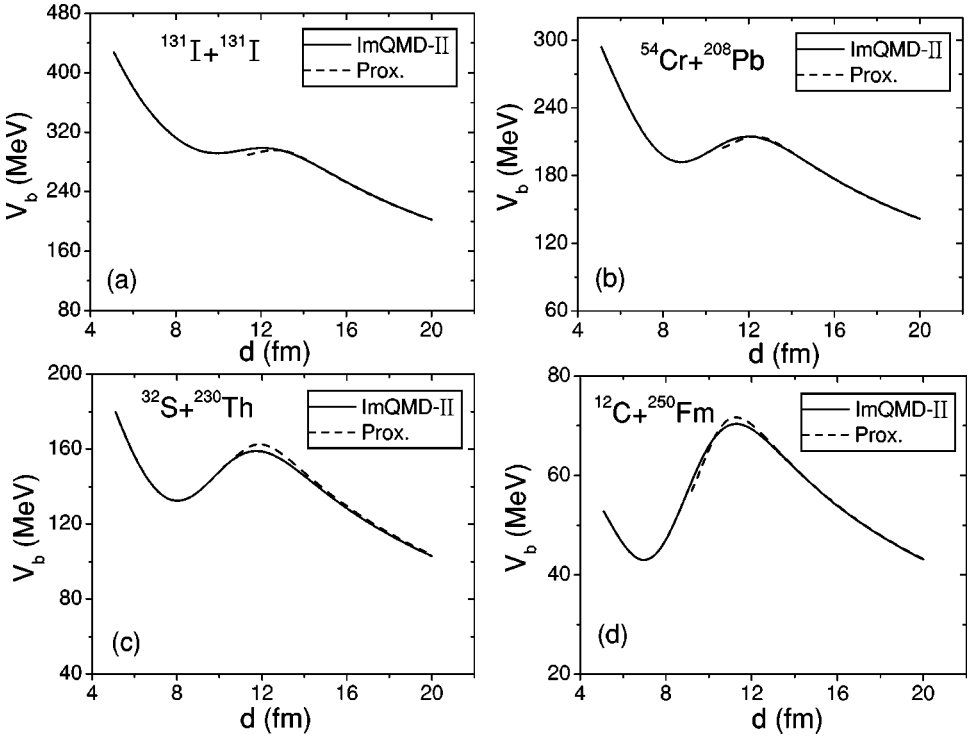

FIG. 3. The static Coulomb barriers of $^{131}I+^{131}I$, $^{54}Cr+^{208}Pb$, $^{32}S+^{230}Th$, and $^{12}C+^{250}Fm$. The solid and dashed curves denote the results of ImQMD-II with parameters of IQ1 and those of proximity potential, respectively.

III. APPLICATIONS TO FUSION REACTIONS NEAR THE COULOMB BARRIER

In this section, we show the calculation results of Coulomb barriers and fusion excitation functions for a series of fusion systems by means of the ImQMD-II model with parameters of IQ1.

A. The Coulomb barrier

The interaction potential $V(R)$ is defined by

$$V(R) = E_{12}(R) - E_1 - E_2. \tag{22}$$

Here R is the distance between the centers of mass of projectile and target. $E_{12}(R)$ is the total energy of whole system, while E_1 and E_2 are the energies of projectile(like) and target(like) part, respectively. For kinetic energies, the Thomas-Fermi approximation is adopted as mentioned in Ref. [26]. By using the ImQMD model, both the static and dynamic Coulomb barrier can be calculated. For the static Coulomb barrier case, the static density distribution which is the same as the initial density distribution of projectile and target is adopted, while for the dynamic Coulomb barrier case the density distribution of the system changes dynamically due to the interaction between the reaction partners.

We show the static Coulomb barriers calculated by the ImQMD-II model with parameter set of IQ1 for $^{40}Ca+^{48}Ca$, $^{40}Ca+^{90}Zr$, $^{16}O+^{16}O$, and $^{16}O+^{208}Pb$ in Fig. 2. The results calculated from proximity potential [27] are also shown in

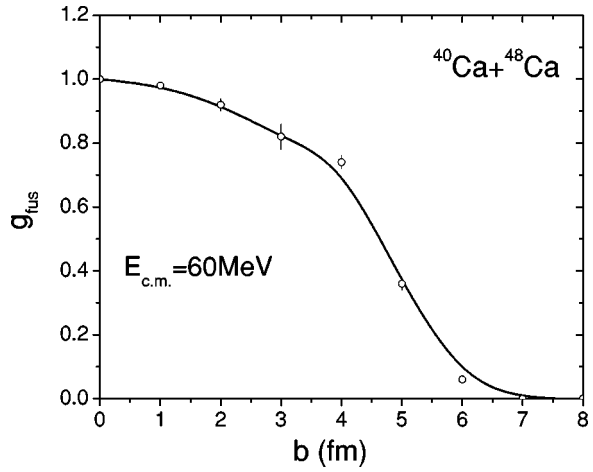

FIG. 4. The probability of fusion reaction $g_{fus}(E,b)$ as a function of impact parameter for $^{40}Ca+^{48}Ca$ at $E_{c.m.}=60$ MeV.

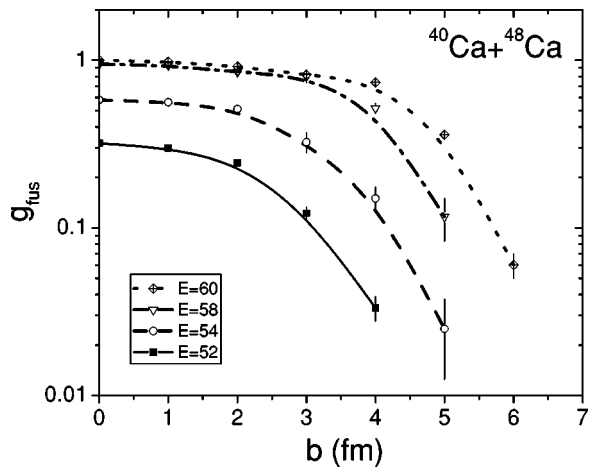

FIG. 5. The probability of fusion reaction $g_{fus}(E,b)$ for $^{40}Ca+^{48}Ca$ at $E_{c.m.}=60,58,54,52$ MeV.

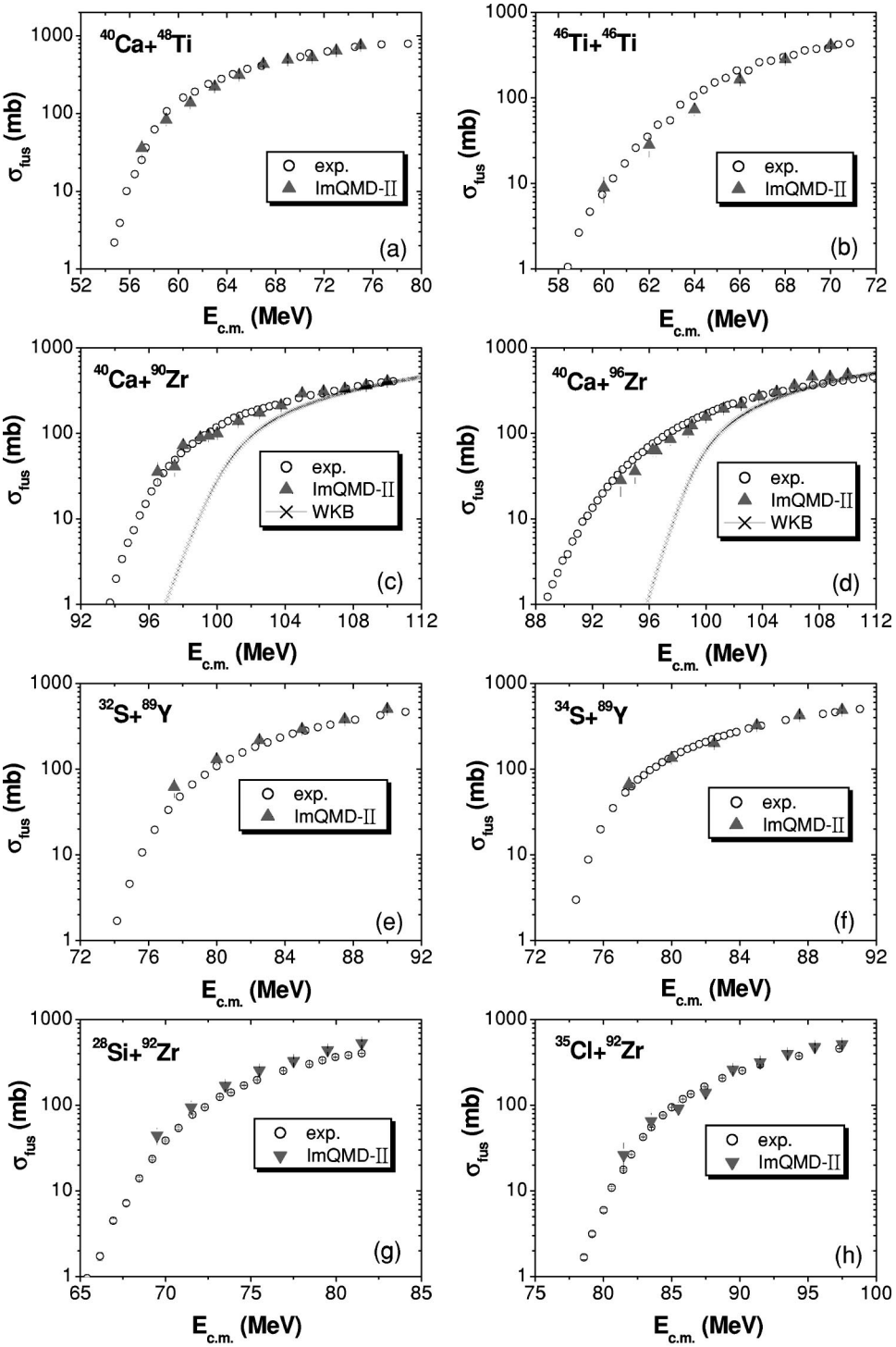

FIG. 6. The fusion excitation functions of (a) ^{40}Ca+^{48}Ti [28], (b) ^{46}Ti+^{46}Ti [29], (c) and (d) ^{40}Ca+^{90,96}Zr [25], (e) and (f) ^{32,34}S+^{89}Y [30], and (g) and (h) ^{28}Si, ^{35}Cl+^{92}Zr [31] at energies near the Coulomb barrier. The open circles denote the experimental data, and the filled triangles denote the results of ImQMD-II with parameters of IQ1. The crosses denote the results of one-dimension WKB approximation.

the figures. One can see that the Coulomb barriers calculated with ImQMD-II are in good agreement with those from proximity potential [27].

In addition, the effects of the mass asymmetry of projectile and target on the static Coulomb barrier are studied through calculating the static Coulomb barriers for ^{131}I+^{131}I, ^{54}Cr+^{208}Pb, ^{32}S+^{230}Th, and ^{12}C+^{250}Fm fusion systems which can form the same compound nucleus ^{262}Sg. In Fig. 3, the solid curves denote the static Coulomb barriers calculated by ImQMD-II with parameters IQ1 and the dashed curves denote the results from the proximity potential. From Fig. 3 one can get two points: the first one is that the results from ImQMD-II are in good agreement with those from proximity potential when two nuclei do not overlap too much in space. The proximity potential may not be able to give an accurate result at the overlapping region where the ImQMD model is applicable. Clearly, the results for the overlapping region are more interesting, especially for the cases of heavy systems. The second one is that with the increase of the mass asymmetry of projectile and target

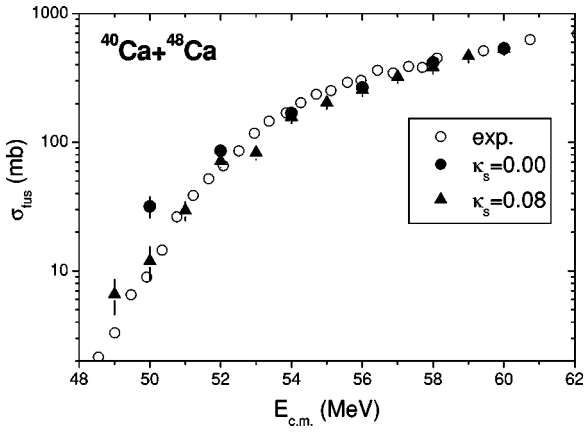

FIG. 7. The fusion excitation function for ^{40}Ca+^{48}Ca. The stars denote the experimental data. The solid circles and triangles denote the results without and with the surface-symmetry term taken into account, respectively.

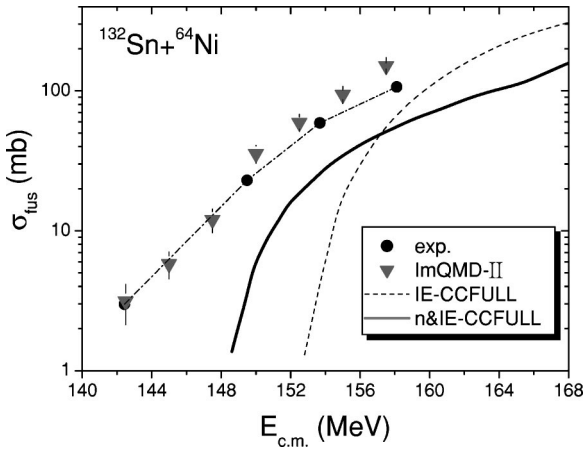

FIG. 8. The fusion excitation function of ^{132}Sn+^{64}Ni [33]. The solid circles denote the experimental data. The filled triangles denote the results of ImQMD-II with parameters of IQ1. The dashed and solid curves denote the results of coupled-channel calculations including inelastic excitation (IE) of the projectile and target and IE plus neutron transfer (n&IE), respectively.

(from ^{131}I+^{131}I to ^{12}C+^{250}Fm) the height of the Coulomb barrier decreases gradually and the capture probability should be enhanced consequently [26].

B. Fusion cross sections

In the ImQMD model, we first create certain reaction events for each incident energy E and impact parameter b (in this work the number is 100) and then counting the number of fusion events, we obtain the probability of fusion reactions, $g_{fus}(E,b)$, then the cross section is calculated by using the expression [3]:

$$\sigma_{fus}(E) = 2\pi \int_0^{b_{\max}} b g_{fus}(E,b) db = 2\pi \sum b g_{fus}(E,b) \Delta b. \tag{23}$$

At a certain incident energy, the probability of fusion reactions $g_{fus}(E,b)$ decreases with the increase of impact parameter as shown in Fig. 4. This is because the interaction between two nuclei decreases gradually from central collisions to peripheral collisions, and following it the probability for fusion reactions decreases and that for elastic scattering processes increases. In addition, the $g_{fus}(E,b)$ decreases quickly with the decrease of incident energies within the energy range interested in this work. Figure 5 presents the evolution of the fusion probability with impact parameter at $E_{\text{c.m.}}=60,58,54,52$ MeV, respectively. One can see from the figure that the fusion probability falls when the incident energy decreases from 60 MeV to 52 MeV and for energies below the Coulomb barrier, fusion events generally only occur at central collisions.

In Fig. 6, we show the fusion excitation functions for ^{40}Ca+^{48}Ti [28], ^{46}Ti+^{46}Ti [29], ^{40}Ca+^{90,96}Zr [25], ^{32,34}S +^{89}Y [30], and ^{28}Si, ^{35}Cl+^{92}Zr [31] at energies near the Coulomb barrier, and the experimental data are also presented for comparison. In the figure the triangles denote the results of ImQMD-II with parameters of IQ1 and the circles denote the experimental data and crosses denote the results of one-dimension WKB approximation [32]. One can see from the figure that calculation results of ImQMD-II for the fusion excitation functions are generally in good agreement with experimental data, which implies that our model is quite reasonable. Now let us study the influence of the surface-symmetry energy term on the fusion cross sections, we show the calculation results of the fusion excitation functions of ^{40}Ca+^{48}Ca [24] at energies near the Coulomb barrier without and with the surface-symmetry energy term taken into account in Fig. 7. One can find from the figure that at incident energies above the Coulomb barrier the fusion cross sections calculated under two cases are approximately equal, while at incident energies below the barrier the difference between two cases become obvious, and for this case the fusion cross sections without surface-symmetry energy term taken into account are obviously larger than the experimental data and those with surface-symmetry energy term taken into account can reproduce the experimental data well. We have found that the N/Z ratio at neck region is enhanced at the early stage for neutron-rich fusion process [4], which is driven by the symmetry potential. It lowers the fusion barrier and consequently enhances the fusion cross section. If only the bulk term is taken into account, the effect of the symmetry energy term becomes too strong at surface region and therefore a surface-symmetry energy term should be taken into account in order to reduce the effect of the bulk symmetry energy term at surface region. It is especially important for having a correct neck dynamics in neutron-rich nuclear fusion reactions.

For further testing the reliability of ImQMD, we calculate the excitation function for fusion reactions of the neutron-rich radioactive beam ^{132}Sn bombarding on the neutron-rich target ^{64}Ni at energies near the Coulomb barrier, which was recently measured [33]. Figure 8 shows the comparison of our calculation results and the experimental data as well as the results from coupled-channel calculations [33]. The solid circles denote the experimental data, the triangles denote the

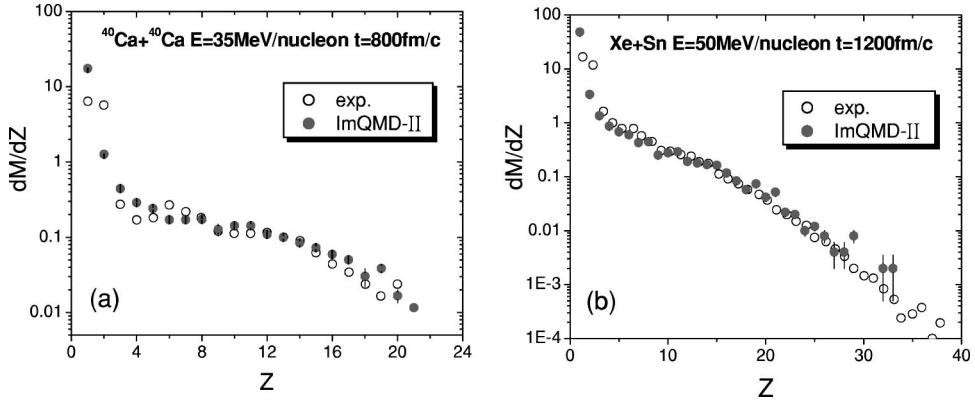

FIG. 9. The charge distribution of fragments for (a) Ca+Ca at $E=35$ MeV/nucleon and (b) Xe+Sn $E=50$ MeV/nucleon. The open circles denote the experimental data, the stars and solid circles denote the results of ImQMD-II model without and with the g_τ term taken into account, respectively. The calculation results are averaged over the impact parameter range of $b=1-3$ fm.

results of ImQMD-II with parameters of IQ1. The dashed and solid curves denote the results of coupled-channel calculations including inelastic excitation (IE) of the projectile and target and IE plus neutron transfer (n&IE), respectively (see Ref. [33] and references therein). From Fig. 8 one can find that the coupled-channel calculations significantly underpredicted the sub-barrier fusion cross sections [33]. This is because with the coupled-channel model it is difficult to consider all degrees of freedom of motion, the number of which is extremely large in sub-barrier fusion reactions for heavier systems, while with the ImQMD model, all degrees of freedom of motion are self-consistently included. Thus, this model may possibly provide us with a useful approach to explore the mechanism of the capture process in the synthesis of superheavy elements. The work concerning this aspect is in progress and the results will be reported in the future work.

As a test we also make applications of our model to describe the charge distributions of fragments in multifragmentation processes. In Fig. 9 we show the charge distribution of fragments by using the ImQMD-II model with parameter set of IQ1 for Ca+Ca at $E=35$ MeV/nucleon [34] and Xe+Sn at $E=50$ MeV/nucleon [35]. One can find that the charge distribution of fragments, especially the number of intermediate mass fragments is in good agreement with experimental data. It is well known that the number of intermediate mass fragments is usually being underpredicted in QMD model calculations. Our results are encouraging and it seems to us that the model can be used for heavy-ion collisions at both low energies and intermediate energies.

IV. CONCLUSIONS AND DISCUSSION

In this work, we have made further improvements in the ImQMD model and proposed a new version, namely, the ImQMD-II model in which a new small correction term and a surface-symmetry energy term are introduced in the potential energy functional in addition to the terms adopted in the normal isospin dependent QMD model. A parameter set for the potential energy functional based on Skyrme interaction of SkM* and SLy series is introduced. By using the new version of the ImQMD model, the ground state properties of a series selected nuclei can be described very well. The time evolution of individual nuclei can remain stable for about several thousands fm/c which roughly fits the requirement for study of fusion reactions of heavy nuclei. We have shown that with this model both the Coulomb barriers and the fusion excitation functions for a series of fusion systems (including neutron-rich radioactive beam ^{132}Sn+^{64}Ni fusion reactions) at energies near the barrier can be reproduced very well. Our study shows that the microscopic dynamical model such as the ImQMD model has an advantage of taking account of the dynamical effects such as the excitations of projectile and target (deformation and vibration), neck formation, isospin, and mass asymmetry, etc. simultaneously and thus offers a useful way to study fusion reactions of heavy nuclei. Furthermore, we have also shown that this model seems to work well on the charge distribution of fragments in multifragmentation processes.

ACKNOWLEDGMENTS

This work was supported by National Natural Science Foundation of China under Grant Nos. 10235030, 10235020, 10175093, and 10175089, and Major State Basic Research Development Program under Contract No. G20000774.

[1] G. G. Adamjan, N. V. Antonenko, W. Sheid, and V. V. Volkov, Nucl. Phys. **A627**, 361 (1997).
[2] K. Hagino *et al.*, Comput. Phys. Commun. **123**, 143 (1999).
[3] Ning Wang, Zhuxia Li, and Xizhen Wu, Phys. Rev. C **65**, 064608 (2002).
[4] Ning Wang, Xizhen Wu, and Zhuxia Li, Phys. Rev. C **67**, 024604 (2003).
[5] Massimo Papa, Toshiki Maruyama, and Aldo Bonasera, Phys. Rev. C **64**, 024612 (2001).
[6] E. Chabanat, P. Bonche, P. Haensel, J. Meyer, and R. Schaeffer, Nucl. Phys. **A627**, 710 (1997); *ibid.* **A635**, 231 (1998).
[7] C. Hartnack *et al.*, Nucl. Phys. **A495**, 303 (1989).
[8] J. Aichelin, Phys. Rep. **202**, 233 (1991), and references therein.

[9] Ch. Hartnack, Rajeev K. Puri, and J. Aichelin, Eur. Phys. J. A **1**, 151 (1998).
[10] A. Ono, H. Horiuchi, Toshiki Maruyama, and A. Ohnishi, Phys. Rev. Lett. **68**, 2898 (1992); Y. Kanada-En'yo and H. Horiuchi, Phys. Rev. C **52**, 647 (1995).
[11] H. Feldmeier and J. Schnack, Rev. Mod. Phys. **72**, 655 (2000).
[12] J. C. Slater, Phys. Rev. **81**, 85 (1951).
[13] C. Titin-Schnaider and P. Quentin, Phys. Lett. **49B**, 397 (1974).
[14] J. Bartel and K. Bencheikh, Eur. Phys. J. A **14**, 179 (2002).
[15] M. Beiner, H. Flocard, Nguyen Van Giai, and P. Quentin, Nucl. Phys. **A238**, 29 (1975).
[16] H. Krivine, J. Treiner, and O. Bohigas, Nucl. Phys. **A366**, 155 (1980).
[17] J. Bartel, Ph. Quentin, M. Brack, C. Guet, and H. B. Hakansson, Nucl. Phys. **A386**, 79 (1982).
[18] J. Dobaczewski, H. Flocard, and J. Treiner, Nucl. Phys. **A422**, 103 (1984).
[19] J. P. Blaizot, Phys. Rep. **64**, 171 (1980).
[20] S. Bjornholm and J. E. Lynn, Rev. Mod. Phys. **52**, 725 (1980).
[21] P. Moller, J. R. Nix, W. D. Myers, and W. J. Swiatecki, At. Data Nucl. Data Tables **59**, 185 (1995).
[22] P. Danielewicz, nucl-th/030105.
[23] D. Vautherin and D. M. Brink, Phys. Rev. C **5**, 626 (1972).
[24] M. Trotta *et al.*, Phys. Rev. C **65**, 011601 (2001).
[25] H. Timmers, D. Ackermann, S. Beghini, L. Corradi, J. H. He, G. Montagnoli, F. Scarlassara, A. M. Stefanini, and N. Rowley, Nucl. Phys. **A633**, 421 (1998).
[26] V. Yu. Denisov and W. Norenberg, Eur. Phys. J. A **15**, 375 (2002).
[27] W. D. Myers and W. J. Swiatecki, Phys. Rev. C **62**, 044610 (2000).
[28] J. D. Bierman, P. Chan, M. P. Kelly, J. F. Liang, A. A. Sonzogni, and R. Vandenbosch, Physics Laboratory Annual Report, 1995 (unpublished), p. 19.
[29] A. M. Stefanini and L. Corradi, LNL Annual Report, 2000 (unpublished), p. 42.
[30] A. Hukherjee *et al.*, Phys. Rev. C **66**, 034607 (2002).
[31] J. O. Newton *et al.*, Phys. Rev. C **64**, 064608 (2001).
[32] C. Y. Wong, Phys. Rev. Lett. **31**, 766 (1973).
[33] J. F. Liang *et al.*, Phys. Rev. Lett. **91**, 152701 (2003), and references therein.
[34] K. Hagel *et al.*, Phys. Rev. C **50**, 2017 (1994).
[35] S. Hudan *et al.*, Phys. Rev. C **67**, 064613 (2003).